Global Reaction Route Mapping on Potential Energy Surfaces of Formaldehyde, Formic Acid, and Their Metal-Substituted Analogues

Koichi Ohno* and Satoshi Maeda

Department of Chemistry, Graduate School of Science, Tohoku University, Aramaki, Aoba-ku, Sendai 980-8578, Japan

Received: February 22, 2006; In Final Form: May 19, 2006

Global reaction route mapping of equilibrium structures, transition structures, and their connections on potential energy surface (PES) has been done for MCHO (M = H, Li, Na, Al, Cu) and HCO_2M (M = H, Li). A one-after-another technique based on the scaled hypersphere search method has been successfully applied to exploring unknown chemical structures, transition structures, and reaction pathways for organometallic systems. Upon metal substitution, considerable changes of stable structures, reaction pathways, and relative heights of transition structures have been discovered, though some features are similar among the analogues. Al and Cu atoms were found to behave as very strong scissors to cut the CO double bond in MCHO. Energy profiles of the CO insertion into Li−H and Li−CH_3 bonds were found to be very similar, especially around the structures where the Li atom is not directly connected with the methyl group, which indicates little effects of alkyl substitution on the reaction route topology.

1. Introduction

It is of great significance to know all chemical structures (isomers) producible from a given atomic constitution corresponding to a particular chemical formula. The following questions are also interesting problems, how the isomers can be converted into one another, and how they can decompose into smaller species, or conversely how they are made of smaller species. These questions can be solved in principle theoretically from the potential energy surface (PES);[1−3] (a) an individual equilibrium structure (EQ) on PES corresponds to a chemical species, (b) a first-order saddle point on PES, a maximum along only one direction and a minimum for all other perpendicular directions, is called a transition structure (TS), which connects the reactant with the product via minimum energy paths or intrinsic reaction coordinates (IRC),[4] and (c) a valley leading to fragment species is denoted as a dissociation channel (DC). Global reaction route mapping (GRRM) is required to elucidate overall reaction pathways including EQ, TS, and DC.

GRRM based on theoretical analyses has not been performed except for systems with only a few atoms, since a fine-tooth comb test of mathematical conditions in the multidimensional coordinate space encounters an obstacle due to heavy computational demands. Even a system of only five atoms ($N = 5$) requires tremendous times of calculations because of high dimensionality of the normal coordinate space ($3N - 6 = 9$).

Conventionally, EQ and TS have been searched by geometry optimization techniques such as rational function optimization (RFO)[5] or the geometry direct inversion in iterative subspace (GDIIS)[6] method. Although these methods are excellent for finding the nearest stationary point from the initially assumed geometry, the obtained structure depends decisively on the initial guess. The eigenvector following (EF) technique[7−12] can locate a stationary point by uphill walking on PES from EQ toward an eigenvector direction of normal-mode analyses. A choice of intermediate directions can be used to improve the EF method.[13] Although some TS points are on the side of the valley floor and cannot be found directly,[3] additional searches from found TS points considerably improve the performance of the EF method.[14] A gradient extremal following (GEF) method tracing the gradient extremal point on the constant energy constraint from an EQ[7,15−23] is another surface-walking technique, though there is an example where an EQ is isolated in GEF path connections.[22] The GEF method has been applied to the ab initio PES of formaldehyde (HCHO) at the HF/STO-3G level of calculations,[23] and the first systematic global analysis of ab initio PES has been made for a system of more than three atoms. More recently, a reduced gradient following (RGF) technique[24−29] was applied to HCHO at the level of HF/STO-3G.[24] By the RGF method, some new EQ corresponding to van der Waals complexes with weakly bound structures were found additionally. In these EF, GEF, and RGF methods, $2(3N - 6)$ pathways should be traced from all stationary points to complete global analyses. It has been pointed out that these methods do not necessarily connect neighboring stationary points.[3]

To make GRRM, random trials or repetitions of trial and errors are not suitable for the following reasons. There is no guarantee of reaching the final stage of the search within finite trials. There may be many duplicated trials around the same regions. Although use of intuition or some chemical knowledge as well as artificial limitations may be successful for some limited cases, such an approach will not be effective in general for uncultivated regions on PES. Thus, a technique following reaction routes is recommended for GRRM, because a general reaction-route following technique would enable us to trace all reaction routes one after another within finite processes. If TS is discovered, then one can go down from TS to EQ or DC along minimum energy paths by a downhill technique such as the steepest-descent method. On the other hand, uphill walking along a reaction route from EQ toward TS or DC had long been the major obstacle for performing GRRM, since an efficient

* Author to whom correspondence should be addressed: E-mail: ohnok@qpcrkk.chem.tohoku.ac.jp.

10.1021/jp061149l CCC: $33.50
Published on Web 06/16/2006

search of the initial directions of reaction routes starting from EQ had been impossible.

Newton trajectories (NT) have been employed to extract characteristic features of reaction paths on PES,[30] and this method is applied to finding reaction channels for H_2O and HCHO, although a general procedure of its application to GRRM has not been established. Recently, the authors have proposed the scaled hypersphere search (SHS) method as a new uphill walking method by noting anharmonic downward distortions of PES, which in combination with a conventional downhill walking technique enables us to follow reaction routes one after another.[31,32] Although in these studies basic properties of the SHS method have been compared with available global reaction route maps for a benchmark system of HCHO by the GEF method[23] and the RGF method,[24] further applications should be made to know the general performance of the SHS method. For example, metal-substituted formaldehyde, MCHO, can be the most suitable system in connection with the benchmark studies on HCHO.[23,24] In addition, HCOOM can also be an interesting system to study, since extensive studies on reaction routes have been made for HCOOH for more than two decades by many groups;[33−35] separate investigations have been made for the water-gas conversion, the isomerization[33] and decomposition[34] of formic acid, reactions in atmosphere for some peroxide isomers.[35]

In this paper, we describe the significance of the anharmonic downward distortion of PES in connection with the SHS method for GRRM. Performance of the SHS method is studied by its applications to (1) MCHO with (M = H, Li, Na, Al, Cu), similar systems with different metal substitution, (2) H_2CO_2, a typical organic system with normal valency, as well as HCO_2Li, an organometallic system with a metal atom having a hypervalent character.

2. One-After-Another Method for Global Reaction Route Mapping

2.a. Chemical Features of Potentials and Anharmonic Downward Distortions. To elucidate reaction routes globally on the PES for a given atomic composition corresponding to a certain chemical formula, a technique for uphill walking must be developed. Although downhill walking for searching an equilibrium structure EQ can easily be done by conventional geometry optimization methods or the steepest descent method, a general uphill walking method starting from an EQ has not been established for searching another EQ (via a transition structure TS) or a dissociation channel DC.

For this purpose, one should study chemical characteristics of potential energy curves around an EQ point on going to a dissociation channel DC or bond dissociation (Figure 1A) as well as a reaction pathway leading to another equilibrium EQ′ via TS corresponding to bond reorganization (Figure 1B). Associated with bond dissociation or bond formation, there is a potential well with a long-range flat curve leading to dissociation or a short-range steep repulsive wall due to very strong repulsion over the short distance. Potential energy curves for diatomic systems, such as Morse potential and Lennard-Jones potential,[2] have the common feature as shown in Figure 1A. Interference of neighboring chemical structures generally leads to an avoided crossing of a pair of parabolic curves as shown in Figure 1B. Such a landscape via a mountain pass or a transition structure TS is in general a prototype of reaction routes connecting a reactant EQ and a product EQ′. It is well-known that a transition structure is related to the interplay of potentials around the reactant and the product. This tendency has been used in the theories or postulates of Bell,[36] the Evans and Polanyi principle,[37] the Hammond postulate,[38] the Woodward−Hoffmann rule,[39] the frontier orbital theory by Fukui,[40,41] and the Marcus equation.[42]

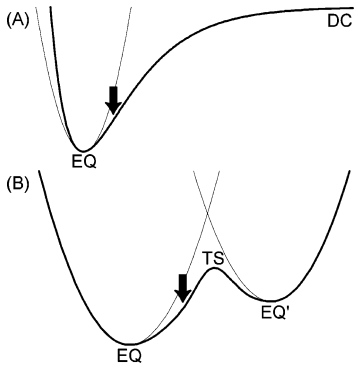

Figure 1. Characteristic features of typical potential energy curves for chemical reactions: (A) a potential energy curve for bond creation−destruction, corresponding to a dissociation channel (DC) starting from an equilibrium structure (EQ) and (B) a potential energy curve for bond reorganization, related to an avoided crossing of two parabolic potential wells centered at EQ and EQ′, which yields a transition structure (TS) around the crossing point. Anharmonic downward distortion (denoted by thick sold arrow) of the real potential from the harmonic potential (parabola shown by thin lines) centered at an equilibrium structure (EQ) indicates a symptom of chemical reactions toward other chemical species via the dissociation channel (DC) or the transition structure (TS).

The common feature of reaction routes starting from an EQ point can be summarized as anharmonic downward distortions (ADD) as indicated by arrows in Figure 1A,B. The existence of DC necessarily flattens the potential curve over the long distance. The existence of another equilibrium point EQ′ around an EQ causes a quantum mechanical avoided crossing of two parabolic surfaces to produce a saddle. Such tendencies due to the existence of neighboring EQ or DC affect the local properties of potentials around an EQ. Thus, ADD around an EQ point can be considered as symptoms of chemical reactions on PES. Since this is the common trend for both bond creation−destruction and bond reorganization, which are results of quantum mechanical interactions of constituent atoms, one may refer to this propensity as the quantum principle of chemical reactions. This provides a fundamental basis for uphill walking along reaction routes departing from an EQ point on PES.

2.b. Scaled Hypersphere Search (SHS) Method. Initial directions of reaction routes from an EQ can be found as local maxima of ADD among all directions in the full coordinate space. Although ADD may be detected as negative third-order terms in the Taylor expansion of the potential at EQ, searching for maximal directions of absolute third-order derivatives is difficult. When one compares energy values of a real PES with the hypothetical harmonic values, local maxima of ADD can be determined easily. The isopotential energy contour for the harmonic potential becomes an ellipsoidal hypersurface, which can be used as a reference surface. In other words, directions of maximal ADD can be found as real energy minima on the reference surface on which every point should have the same energy when the potentials are harmonic. This strategy is more favorable than using higher order derivatives. Limitation of the searching space within the closed region also has a great advantage to avoid endless procedures.

Comparison of a real PES with the reference harmonic surface may be made by use of any coordinate system. If one employs the scaled (reduced) normal coordinates defined by $\boldsymbol{q}_i = \lambda_i^{1/2}\boldsymbol{Q}_i$,

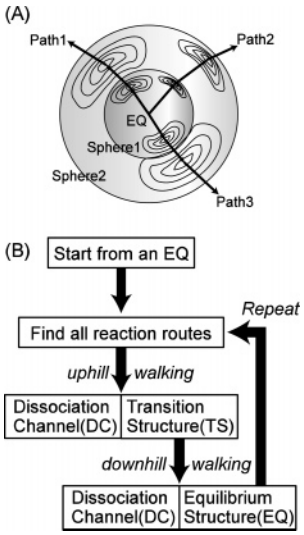

Figure 2. Schematic illustrations of computational procedures for GRRM by the SHS method: (A) Though the reference harmonic potential has a constant energy on the scaled hypersphere surface, the real potential has some minima on the same surface, which correspond to the anharmonic downward distortions indicating the symptoms of chemical reactions. Following those minima on different sizes of scaled hypersphere (spheres 1 and 2), reaction routes (paths 1−3) can be traced from the equilibrium structure (EQ) by the SHS method as shown by arrows. (B) Starting from an EQ, find all reaction routes as energy minima on the scaled hypersphere (maxima of anharmonic downward distortions), then continue uphill walking to reach DC or TS, and then downhill walking from the TS region to DC or another EQ. From each new EQ, the above procedures for finding DC, TS, and EQ should be repeated until no new EQ is found. This one-after-another approach in the SHS method can be automated, and it enables us to perform GRRM within finite processes.

where $\boldsymbol{Q}_i$ is a normal coordinate with a respective eigenvalue λ_i,[31,43] every direction can be treated equivalently, and the reference isoenergy hypersurface becomes a simple hypersphere. In this representation, one needs not to determine the shape of the isoenergy hypersurface in the multidimensional space, and the harmonic energy value on the hypersphere can be automatically obtained from the distance from the EQ point, which means that, for optimization finding maximal ADD, real potential energy values can be used directly rather than use deviations from the reference harmonic values.[31,32] Although the SHS method initially seemed to be limited to a certain short range from EQ, namely at most to the neighboring TS regions, it works excellently even in the neighboring EQ regions, because the neighboring potential well appears as an energy minimum on the scaled hypersphere.[44]

In the SHS method, the following procedures are made around an EQ. (1) At an EQ for a given chemical composition, normal coordinates are determined at first. (2) Around the EQ, PES is expanded in terms of scaled normal coordinates. (3) Reaction path points (SHS path points) are determined as energy minima on a scaled hypersphere with a center fixed at the EQ. (4) By using several sizes of hypersphere, one can obtain a series of points for the pathways around the EQ, as schematically shown in Figure 2A. These paths can be denoted as SHS paths. (5) An indication of a TS region can be obtained from variation of first order derivatives along SHS path points. The location of each TS can be determined precisely by an application of a conventional technique in the TS region.[5,6] (6) Asymptotic behavior separating a fragment from the remaining part indicates a DC. Further details of the SHS method will be described in the following sections.

2.c. Energy Minimization on the Hypersphere Finding All SHS Path Points. Although ADD around an EQ can be expected to be searched as individual energy minima on the scaled hypersphere, there are some problems. Energy optimization should be made in a multidimensional hypersurface of $3N - 7$ degrees of freedom for a nonlinear N atom system, and all optimized geometries for local ADD maxima need to be determined. The situation will become complicated if several pathways are nearly overlapping. Energy lowering of neighboring pathways may possibly overlap on the hypersphere, and then downward distortions caused by relatively weak interactions may be obscured or hidden by deeper distortions due to much stronger interactions. It follows that practical techniques are required to be developed for (a) decomposition of overlapped downward distortions into individual components and for (b) efficient energy minimization determining all minima with the least effort.

When energies on the hypersphere of $3N - 7$ degrees of freedom can be constructed from limited numbers of sampled data by a suitable interpolation technique, all minima can easily be obtained. For this purpose we have initially developed a polar coordinate interpolation (PCI) technique[43] based on successive application of one-variable cubic spline procedures to polar coordinates. This PCI technique has been successful in constructing PES efficiently from quantum chemical calculations, and the obtained PES has been applied to GRRM for HCHO.[31] However, the number of required data for the PCI method rapidly increases with the number of normal modes. Thus, we have developed another more efficient algorithm for finding all minima on the hypersphere as described below as the iterative optimization elimination (IOE) method.[32]

To discover overlapped pathways or hidden pathways, a shape function technique is introduced. By using the scaled normal coordinates $\boldsymbol{q} = (q_1, q_2, \ldots q_f)$ for a system with f-degrees of freedom, the potential energy E at a point $\boldsymbol{q}$ is expressed by the following formula.

$$E(\boldsymbol{q}) = \epsilon - \delta(\boldsymbol{q}) \tag{1}$$

Here, ϵ is the reference harmonic value, and $\delta(\boldsymbol{q})$ corresponds to ADD at the position vector $\boldsymbol{q}$. Considering the nature of ADD, δ is replaced by a shape function $G(\boldsymbol{q})$, which is expressed with a cosine function of the angle displacement θ of $\boldsymbol{q}$ with respect to that for the minimum.

$$G(\boldsymbol{q}) = A \cos^3 \theta \qquad (\theta \le \pi/2) \tag{2}$$

Here, A is the depth parameter that is determined as $A = \epsilon - E$ at the minimum. Although the shape function $G(\boldsymbol{q})$ in eq 2 is related to the third-order term in the potential, parameter A includes higher order terms effectively, since A is determined by use of the exact energy value. Since the function value as well as the first and second derivatives of $G(\boldsymbol{q})$ with respect to θ are zero at $\theta = \pi/2$, $G(\boldsymbol{q})$ is continuous up to the second order on the hypersphere. After having obtained a set of shape functions for n individual downward minima, a modified surface, where the initial n minima are eliminated, can be deduced as $E'(\boldsymbol{q}) = E(\boldsymbol{q}) + \sum_{i=1}^{n} G_i(\boldsymbol{q})$. This modified surface $E'(\boldsymbol{q})$ contains hidden downward minima. Local downward minima on this modified hypersphere surface should be searched again. After having found the new n' downward minima, the above treatments should be repeated, until no further hidden minima are discovered. In this manner, this iterative optimization−elimination (IOE) technique[32] yields all minima (SHS path

points) on the hypersphere much more rapidly than the interpolation technique[31] previously used.

2.d. Computational Procedures for GRRM. Here, we summarize the entire procedure for global reaction route mapping (GRRM) of PES by use of the SHS method in combination with IOE and some conventional techniques.

(1) Geometry optimization is made to determine the initial EQ point for a given chemical formula starting from an arbitrary structure. The initial EQ is denoted as EQ0.

(2) Normal-mode-analysis is made at EQ0 to define scaled normal coordinates, with which SHS procedures from EQ0 are made.

(3) The first step of SHS procedures from EQ0 is to find all SHS path points on a scaled hypersphere with a small radius determined from the harmonic vibrational quantum of the softest mode. Uphill walking along SHS paths is made with successively expanded sizes of scaled hypersphere, which provides a series of SHS path points, as shown in Figure 2A.

(4) Minima on the scaled hypersphere, corresponding to the SHS path points, are determined by the IOE technique. Starting points of the minimization procedures, which may be chosen arbitrarily, are systematically selected to be along all normal coordinate directions for rapid convergence to decrease the total distance of minimization walks on the hypersphere. Except for the initial IOE process, starting points on a new hypersphere for iterative IOE processes are guessed from the predictor−corrector projection to save computational demands. If general minimization procedures as the initial IOE are also applied to the subsequent IOE processes, bifurcations of reaction paths, if they exist, can be detected as additional SHS path points.

(5) The above iterative IOE procedures are continued until the SHS pathways reach DC or TS regions. When the nearest interatomic distance between fragments becomes sufficiently larger than a suitable threshold distance such as the summation of van der Waals radii, the pathway can be considered as a DC. Recognition of fragments can easily be made from the interatomic connection matrix made up of 1 or 0 for bonding or nonbonding, which can be produced from the interatomic-distance matrix, whether the distance is smaller or larger than a suitable value estimated from the sum of typical bond radii. Recognition of a TS region can be made from the change of the slope along the pathways. The top of the SHS path can be found as the energy maximum on the SHS path. Refinement of the TS structure is made by a conventional method, such as the RFO method.[5]

(6) From each TS region or the refined structure of each TS, downhill procedures toward both sides are made to determine (or to confirm) the minimum energy path (IRC) until it reaches an EQ or a DC (or returns to the initial EQ), by a conventional downhill technique (the steepest descent method or the second-order method using gradient and Hessian[45]).

(7) Newly discovered TS, EQ, or DC is compared with already found ones. Confirmed new ones are numbered successively as TS*n*, EQ*n*, or DC*n*. This numbering is temporary, since some other conventions may be used in the finally obtained global reaction route map.

(8) After the above procedures (3)−(7) starting from EQ0 are finished, normal coordinate calculations corresponding to process (2) are made for EQ1. Then, the next processes from (3)−(7) are repeated around EQ1 to discover successively TS, EQ, or DC. These cyclic procedures should be repeated for every new EQ, until no unprocessed EQ remains, as is schematically shown as a flowchart in Figure 2B. It should be noted that all reaction routes via TS are confirmed as minimum energy paths (IRC) during the above cyclic procedures.

(9) The above procedures discover entire reaction path connections one after another in a systematic way to yield a global reaction route map for a given chemical composition.

TABLE 1: Number of Gradient and Hessian Calculations To Make GRRM

	gradient	Hessian	no. of EQ	no. of TS
HCHO[a]	7 359	780	5	9
LiCHO[a]	29 706	2 060	8	12
NaCHO[a]	31 461	2 226	10	12
AlCHO[a]	22 570	1 738	10	14
CuCHO[a]	31 743	2 318	11	16
HCOOH[b]	53 780	4 171	12	27
HCOOLi[b]	108 584	7 310	16	27

[a] Calculations by the B3LYP/6-31G level. [b] Calculations by the RHF/6-31G level.

2.e. Computational Details. Computational details are described in the following. In the present study, our homemade program for GRRM procedures was used in combination with a conventional quantum chemical program package.

An original code written by the authors has been used for structure optimizations, normal coordinate analyses, and steepest decent path following processes. Full geometry optimizations were carried out on all EQ and TS points found by the SHS method. For optimizations of EQ and TS points, optimization steps were chosen by use of the size independent RFO (SIRFO) method and the trust radii method (TRM):[46] the TRM steps were used when a SIRFO step exceeded a certain trust radii. For searching EQ, Hessian matrixes evaluated in every 20 steps were updated by the BFGS method.[47] For searching TS, Hessian matrixes evaluated in every 10 steps were updated by Bofill's method.[48] Optimization procedures are considered to be convergent, when the root-mean-square and the maximum force become smaller than 0.00004 and 0.00006 hartree $Å^{-1}$, respectively. Reaction path following was carried out after having found each TS, and this has also been made by use of an original code written by the authors. The steepest descent path is integrated numerically by the second-order algorithm[45] with a step size of 0.1 Å. Since the present purpose of the steepest descent path following is not to determine an accurate reaction path but to confirm path connections, Hessian matrixes evaluated in every 5 steps were updated by Bofill's method in the steepest descent path following.

In the present study, potential energies of MCHO (M = H, Li, Na, Al, Cu) and HCO_2M (M = H, Li) in the singlet ground state were obtained by quantum chemical B3LYP/6-31G and HF/6-31G(d) levels of calculations by using a Gaussian03 program package.[49] The geometries for EQ and TS as well as energies for EQ, TS, and DC were further refined and confirmed at the B3LYP/6-311++G(d,p) level of calculations. When a new EQ happened to be found during confirmation procedures at the higher level, the SHS treatment searching reaction pathways around the particular EQ point was made additionally at the higher level. At each refined EQ or TS point, normal coordinate calculations were made to make zero-point-energy (ZPE) corrections. Relative energies from the most stable isomer of EQ0 in each system including ZPE corrections and ZPE values at the B3LYP/6-311++G(d,p) level of theory are listed in the Supporting Information.

Though it is not easy to describe the cost of the SHS procedures for GRRM, the number of gradients and Hessian calculations to make GRRM were listed for typical cases in Table 1. In the case of the benchmark system of HCHO, the

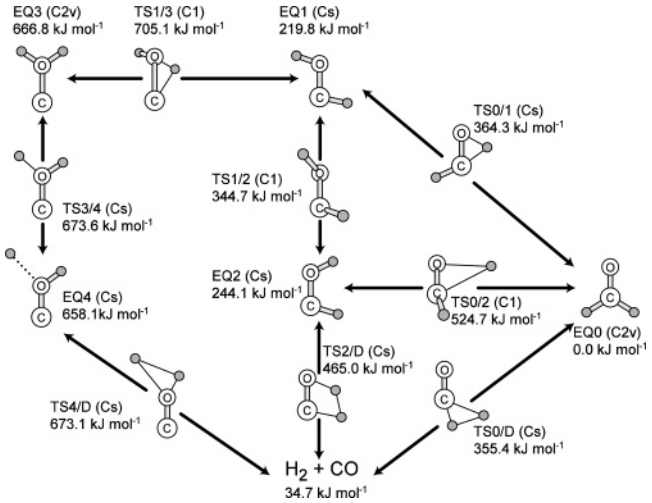

Figure 3. Global reaction route map for HCHO. Isomers (equilibrium structures) and transition structures are denoted by EQ and TS, respectively. Relative energies are shown with respect to the most stable isomer of EQ0. The point group is shown in parentheses. Reaction routes are shown by arrows with a direction to downhill walking.

total numbers of gradients and Hessians were only 7359 and 780, respectively. In the case of metal-substituted systems of MCHO, replacement of H by a metal atom induces the symmetry lowering and increases varieties of stable structures from 5 to 8−11. This increase is nearly double from HCHO to MCHO, thus the number of gradients and Hessian calculations for metal-substituted MCHO become only several times larger than those for the case for HCHO. Among MCHO (M = Li, Na, Al, Cu), computational costs for AlCHO were considerably smaller than the others, probably because the structures are not floppy in good contrast to very floppy characteristics of Li and Na compounds. On going to five atom systems of HCOOH and HCOOLi, the number of gradients and Hessian calculations increased but only by a few factors. In our experiences, the number of gradients or Hessian calculations depends on the third power of the vibrational degree of freedom, which leads to an approximate estimate of ca. $\{(3 \times 5 - 6)/(3 \times 4 - 6)\}^3 = 3.4$, which is comparable with ratios for (HCOOM) vs (MCHO). The SHS procedures for GRRM have been successfully applied to a seven-atom system,[32] and the present level of techniques for GRRM can also be applied to the larger systems of 10−12 atoms, for which GRRM calculations are in progress.

3. Results and Discussion

3.a. MCHO. Four-atom systems of MCHO (M = H, Li, Na, Al, Cu) were chosen to compare GRRM for a series of similar systems with different metal substitution. HCHO is a benchmark system that has been studied by the GE method,[23] the RGF method,[24] as well as the SHS method.[31,32] Concerning the metal-substituted MCHO, the CO insertion reaction into M−H or M−CH_3 bonds, for a transition metal or a transition metal complex M, has been studied extensively in connection with transition metal mediated catalytic cycles,[50−52] although there are few reports concerning reactions in MCHO (M = Li, Na, Al, Cu) systems except for a few studies for $MCCH_3O$ (M = Li,[53] Na[54]) systems.

Global reaction route maps for MCHO (M = H, Li, Na, Al, Cu) are shown in Figures 3−7. In these figures, simple channels dissociating into two radicals are omitted. All reaction routes were confirmed to be minimum energy paths during the GRRM procedures. An isomer (equilibrium structure) is denoted as EQ*n*,

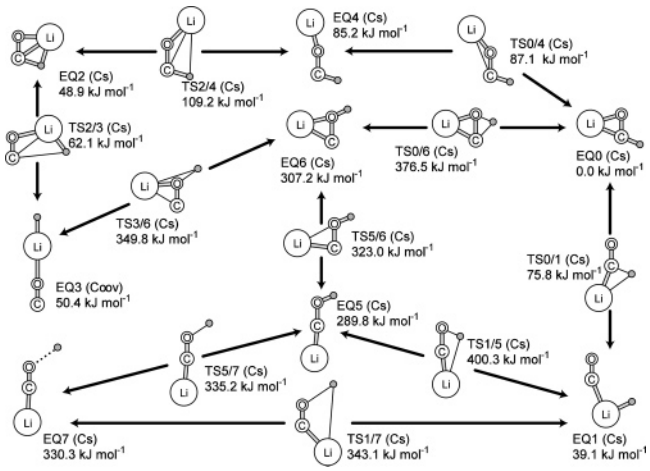

Figure 4. Global reaction route map for LiCHO. Notations are the same as those in Figure 3.

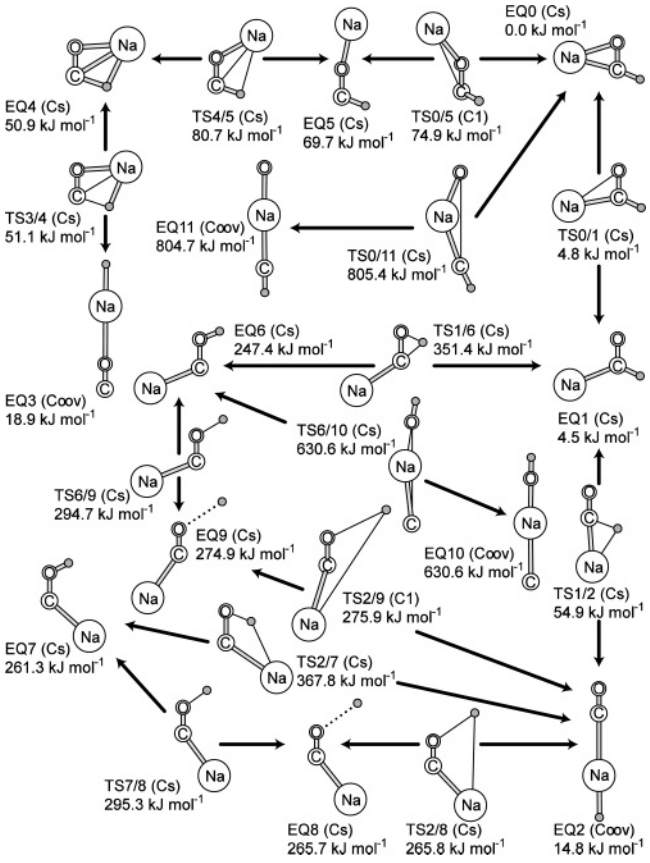

Figure 5. Global reaction route map for NaCHO. Notations are the same as those in Figure 3.

a TS between EQ*n* and EQ*m* is shown as TS*n*/*m*, and a TS connecting EQ*n* with a DC is labeled by TS*n*/D. Transition structures TS*n*/*n* returning to the same form are omitted, because such a TS is meaningless as a chemical reaction route connecting different species. For each EQ or TS, the point group is labeled in parentheses, and the relative energy is shown with respect to the most stable isomer specified as EQ0. Obtained EQs were numbered from the lowest according to the energies, irrespective of the temporary numbering in the searching procedures. This convention for the numbering in the global map is used throughout this study. The ZPE correction was not made in Figures 3−7. Each reaction route is shown by an arrow with a

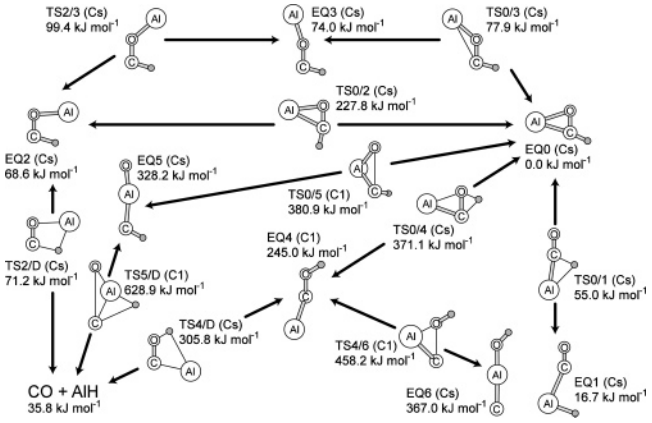

Figure 6. Global reaction route map for AlCHO. Notations are the same as those in Figure 3.

direction to downhill walking. Structures are shown with ball-and-stick models, and metastable bonds in TS are shown by thin lines.

A comparison of GRRM in Figures 3−7 and interesting physical arguments can be summarized as follows.

(1) Structures similar to the most stable isomer of HCHO (EQ0 in Figure 3) with a formyl group (CHO) can only be found in NaCHO (EQ1 in Figure 5) and CuCHO (EQ1 in Figure 7), and no such structures are found for LiCHO (Figure 4) and AlCHO (Figure 6), for which the most stable structures (EQ0) involve a three-membered ring with a divalent O−M−C bridge (M = Li, Al). These differences can be related to the magnitude of the s−p gaps, which are much smaller for Li and Al to result in strong electron donating interaction from a metal p-orbital into an antibonding pseudo-π-orbital at the CO unit. A population analysis shows that the local charge on the Li atom is +0.86 in EQ0 of Figure 4, which indicates strong electron donation from the metal atom to the CO unit. In the case of NaCHO, a ring structure with a bridged form of O−Na−C is most stable, whereas in CuCHO, a linear structure of HCuCO is most stable because of the strong interaction[55−57] between Cu and C. Two types of ring structures are found for O−Li−C with a H atom attached on either the O or C side.

(2) The cis−trans isomerization pathways in H−O−C−H (EQ1−EQ2 in Figure 3) are retained in Figure 6 (EQ2−EQ3: Al−O−C−H) and Figure 7 (EQ6−EQ5: Cu−C−O−H and EQ3−EQ4: Cu−O−C−H), though other types could not be found. Although the cis−trans isomerization pathways in Na−C−O−H (EQ6−EQ7 in Figure 5) have also been found on lower levels of PES, it could not be located on the B3LYP/6-311++G** level of PES because of the limitation of the restricted single-determinant SCF calculations around the corresponding region of the PES. The origin of the cis−trans isomerization in HCHO is the sp^2 hybridization at the C and O atoms that inhibits the rotation along the CO axis. In HCHO, there are two channels for the cis−trans isomerization, as reported in previous studies;[23,24,31,32] the out-of-plane rotation of the OH group around the CO axis, and the intraplane rotation of the CH group. Between these two pathways, the barrier height of the intraplane rotation is much larger than that of the out-of-plane rotation. This propensity is also clearly retained in the comparison between the out-of-plane route EQ6−EQ5 of Cu−C−O−H and the intraplane route EQ3−EQ4 of Cu−O−C−H. Whereas for other cases, intraplane rotations of metal atoms around the CO unit become easier to tend to form ring structures using a p-orbital of the metal atoms.

(3) Two types of chain structures of H−M−C−O and H−M−O−C can be found for M = Li, Na, and Cu, but only H−M−C−O is found for M = Al. It should be noted that H−Li−C−O (EQ1 in Figure 4) and H−Al−C−O (EQ1 in Figure 6) have considerably bent structures, whereas others are linear. This tendency can be related to the strong activities of the p-orbitals of Li and Al atoms.

(4) Stable inserted structures of C−M−O−H and O−M−C−H are found for M = Al, Cu, whereas for M = Li, Na only kinetically very unstable structures can be seen (in the case of M = Li, both linear structures of C−Li−O−H and O−Li−C−H have been found to be second-order saddles). Although population analyses revealed that C−M−O−H and O−M−C−H are commonly ionic, relative heights of transition states are considerably different. As can be seen in Figure 5, the barrier heights for C−Na−O−H and O−Na−C−H are both very low to decompose into the more stable structures with the CO unit easily. On the other hand, for Al and Cu compounds, sufficiently high barriers appear as TS0/5, TS5/D, and TS4/6 for Al in Figure 6 as well as TS5/7, TS7/10, and TS1/9 for Cu in Figure 7. Kinetic stability of the metal inserted structures into the CO unit may lead to possibilities to react with some other species. Thus, this tendency suggests that Al and Cu atoms may behave as strong scissors to the CO double bond, although very large activation energies of 213 (Al) and 313 (Cu) kJ mol^{-1} are required for insertion reactions.

The above features are found to be peculiar to respective metal atoms, and these characteristics are interesting in considering reaction routes for organometallic systems. In connection with this topic, additional studies were made for a reaction route for the reaction of RLi (R = H, CH_3) with CO. In Figure 4 a series of reactions (EQ1−TS0/1−EQ0−TS0/4−EQ4−TS2/4−EQ3−TS2/4−EQ2−TS2/3−EQ3) for R = H (LiCHO) are included, which are also shown in Figure 8. As shown in Figure 8, energy profiles of the reaction routes for the methyl-substituted system (R = CH_3) were found to be very similar with those for R = H, especially around the structures where the Li atom is not directly connected with the methyl group. It follows that GRRM for simpler systems may be helpful in studies on the larger organic systems with the same functional groups or very similar chemical structures.

3.b. H_2CO_2 and HCO_2Li. Figures 9 and 10 show global reaction route maps in the singlet ground state for H_2CO_2 and HCO_2Li obtained by the SHS method in the present study. All reaction routes in Figures 9 and 10 were confirmed to be minimum energy paths during the GRRM procedures. Notations such as EQ*n*, TS*n*/*m*, and TS*n*/D are the same as those in Figures 3−7. van der Waals complexes (H_2 + CO_2, H_2O + CO) are shown as dissociated products with energies at the dissociation limit. Simple DCs yielding atomic fragments are excluded for simplicity, though DCs producing two stable molecules (LiH + CO_2, LiOH + CO) are shown explicitly. The ZPE correction was not made in Figures 9 and 10. The maps are divided into two regions: (1) the acid region is composed of low-energy isomers (lower than 240 kJ mol^{-1}) including EQ0 (0 kJ mol^{-1}) and (2) the peroxide region contains high-energy isomers (higher than 390 kJ mol^{-1}). The latter regions are shaded.

The global map for H_2CO_2 in Figure 9 includes the water-gas conversion H_2O + CO → H_2 + CO_2, the isomerization of formic acid HCOOH (EQ0, EQ1) into dihydroxycarbene HO-COH (EQ2, EQ3, EQ4), unimolecular decomposition processes of HCOOH into H_2O + CO or H_2 + CO_2, reactions in the atmosphere including dioxirane OCH_2O (EQ5) as well as various peroxides, H_2COO (EQ7), HCOHO (EQ11, EQ12), and

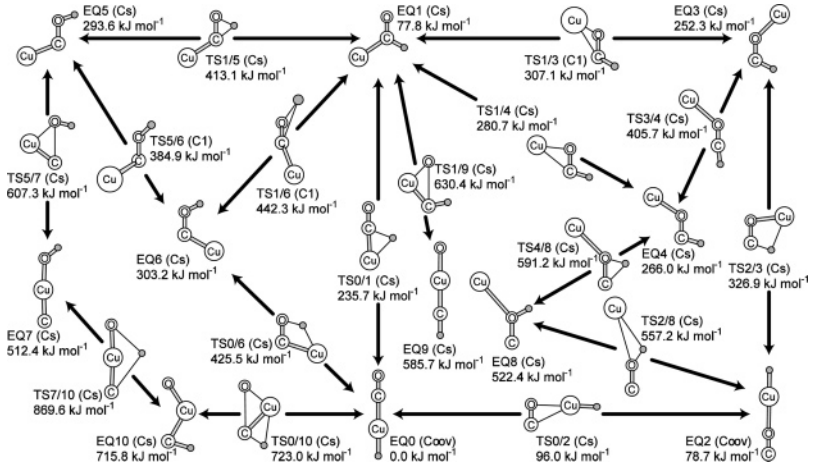

Figure 7. Global reaction route map for CuCHO. Notations are the same as those in Figure 3.

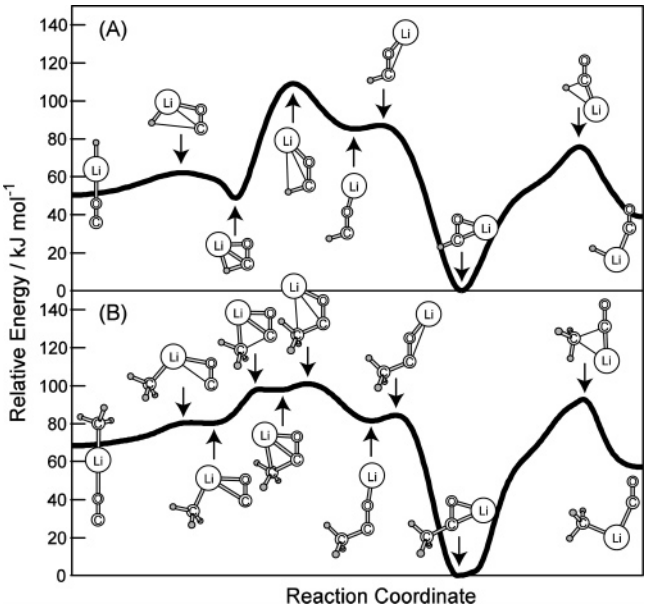

Figure 8. Energy profiles of the reaction of RLi (R = (A) H, (B) CH_3) with CO.

HC−O−OH (EQ6, EQ8, EQ9, EQ10). In addition to these reaction pathways so far studied extensively for more than twenty years, new transition structures of TS0/10, TS1/8, and TS2/11 connecting acids and peroxides have been discovered in the present study. It follows that the SHS method performs GRRM to elucidate unknown reaction routes systematically without experience or intuition.

Unimolecular dissociation processes producing stable molecules such as $H_2O + CO$ or $H_2 + CO_2$ are very important since such processes can be used as synthetic routes without byproducts. In the case of H_2CO_2, several reaction pathways were found via TS0/D, TS3/D, TS6/D for $H_2O + CO$ and TS1/D, TS4/D, TS5/D for $H_2 + CO_2$. Such kinds of reaction routes are especially important for describing how to produce a chemical compound by direct synthesis without unwished byproducts satisfying the perfect efficiency of the atom economy recommended for sustainable chemistry or green chemistry.[58−61]

Considering ZPE corrections and the very low barrier heights, some peroxides (HC−O−OH) of EQ6, EQ8, and EQ10 are kinetically unstable. Two isomers of HCOHO, EQ11, and EQ12 are considered to be metastable. Conversion between two isomers of formic acid (EQ0 and EQ1) may easily occur. All other isomers are considered to be kinetically stable. As can be seen from the acid region including dihydroxycarbenes (HO-COH), the lowest energy route for the water-gas conversion $H_2O + CO \rightarrow H_2 + CO_2$ is confirmed to be a pathway via TS0/D−EQ0−TS0/1−EQ1−TS1/D. Some other routes via EQ3 and EQ4 may also be important, because the TS energy levels at ca. 333−346 kJ mol^{-1} are only slightly higher than that of TS1/D (307 kJ mol^{-1}). Direct fixation of CO_2 with H_2 into formic acid in the gas phase proceeds via TS1/D.

Among the peroxides, EQ5 and EQ7 will have longer lives in atmospheric environment. Among four isomers of HC−O−OH, EQ8, EQ9, and EQ10 are almost instantaneously converted into formic acid, whereas EQ6 readily dissociates into $H_2O + CO$. Conversion from acids into peroxides is difficult, because of the very high energy barriers of 513−913 kJ mol^{-1}. Among the total 30 TS, there are 13 TS with cyclic structures including a single H atom, and 3 TS (TS1/D, TS4/D, TS5/D) have a H−H bridge leading to $H_2 + CO_2$. No substantial bond breaking is found for TS0/1, TS2/3, TS3/4, TS2/4, TS6/8, TS8/9, and TS11/12. The COO ring is found for TS0/10, TS1/8, TS8/10, TS2/11, TS10/11, TS10/12, TS6/10, TS5/7, TS5/10, and TS5/D. It is of note that acids and peroxides are connected via the COO ring structure.

In Figure 10 the global map for HCO_2Li can also be divided into acid and peroxide regions. The peroxide region is shaded as in the case of H_2CO_2. Remarkable differences from the map for H_2CO_2 can be summarized below by using state labels of EQ*n*(H) or TS*n*/*m*(H) for H_2CO_2 and EQ*n*(Li) or TS*n*/*m*(Li) for HCO_2Li.

(a) Hypervalency of Li atoms[62] causes drastic changes in the reaction route map. Except for EQ7(Li), the Li atom locates its position at a multibonded site, while the H atom in EQn(H) is mostly found at a terminal bond of OH or CH type. In EQ2-(Li), EQ3(Li), and EQ6(Li), the Li atom occupies a divalent position with a linear geometry.

(b) Lithium formate, HCOOLi, which can easily be converted into formic acid by hydration, has a unique structure of EQ0-(Li) in contrast to the trans-form EQ0(H) and cis-form EQ1(H) for formic acid. No other acid structure with a CH bond exists for HCO_2Li.

(c) The dioxirane structure of EQ5(H) as an important peroxide and a cis-type isomer of dihydroxycarbene of EQ4-(H) as an important intermediate for CO_2 fixation are missing for HCO_2Li.

(d) A conversion route for $LiOH + CO \rightarrow LiH + CO_2$ corresponding to the water-gas conversion of $H_2O + CO \rightarrow H_2$

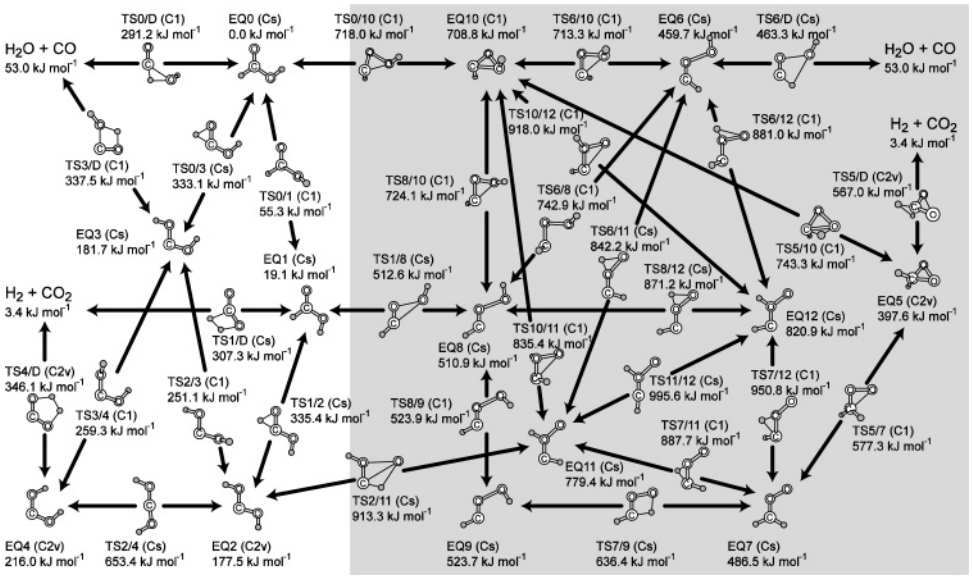

Figure 9. Global reaction route map for H_2CO_2. Trans (EQ0) and cis (EQ1) isomers of formic acid HCOOH are included in the lower energy region, whereas peroxides such as dioxirane (EQ5) exist in the higher energy region shown by the shade. Other notations are the same as in Figure 3.

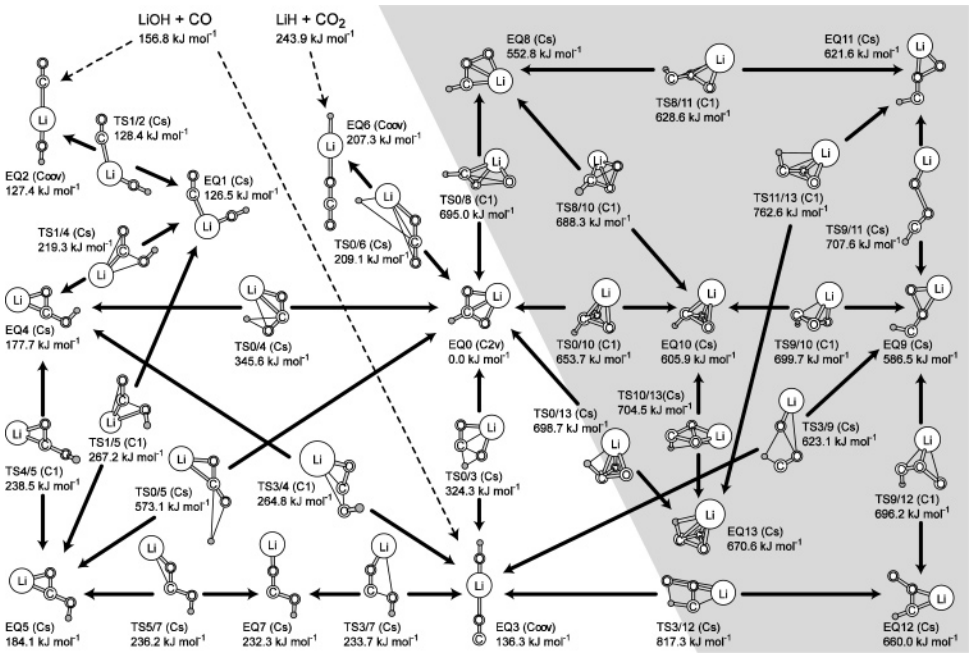

Figure 10. Global reaction route map for HCO_2Li. Lithium formate HCOOLi is the most stable isomer (EQ0). Dashed lines indicate direct dissociation pathways from EQ without TS. Other notations are the same as in Figure 3.

+ CO_2 can be seen as EQ3(Li)−TS0/3(Li)−EQ0(Li)−TS0/6(Li)−EQ6(Li). The CO_2 fixation pathway to EQ0(Li) via EQ6(Li) should be noted,[63] because this route is almost barrier free from the dissociated level of LiH + CO_2. No conversion pathways from CO or CO_2 to each other are found via peroxides for HCO_2Li.

(e) All peroxides have very high energy levels of 553−671 kJ mol^{-1} with respect to HCOOLi EQ0(Li). Once the highest energy peroxide of EQ13(Li) is produced in the gas phase, then it will be readily converted into HCOOLi via TS0/13(Li) to produce other isomers with the CO_2 skeleton because of the excess energy, enough to pass over relatively low TSs in the acid region.

It should be noted that the quantum principle of chemical reactions noting the anharmonic downward distortion works well in the SHS method, even though many subtle bonds are included in a metal-containing system. Remarkable changes of reaction pathways upon replacement of a hydrogen atom by a lithium atom indicate the significance of the microscopic roles of a metal atom on the reaction routes in connection with the catalytic behavior of metals.

4. Concluding Remarks

The SHS method provides a useful means to perform GRRM and to elucidate chemical species producible from a given set of atoms and their chemical reaction routes. This approach is especially important for single molecule reactions or unimolecular processes such as intramolecular hydrogen transfer as well as building block synthesis of molecules without

byproducts. Discovery of dissociation channels in GRRM indicates the reverse reaction process synthesizing the initial species from the dissociated fragments,[64,65] which tells us the method to produce a chemical compound by direct synthesis without unwished byproducts satisfying 100% efficiency of the atom economy recommended for sustainable chemistry or green chemistry.[58−61]

GRRM based on the quantum principle of chemical reactions can proceed automatically until it terminates within finite processes following anharmonic downward distortions as symptoms of chemical reactions. GRRM will be explored extensively for much larger systems by supercomputer systems. One of the outstanding advantages of the SHS method is that it can be used without chemical insight or intuition, since the SHS method itself pays attention to symptoms of chemical reactions (anharmonic downward distortions of PES). The SHS method for GRRM opens a new window on the chemical world by combining sophisticated quantitative quantum chemical methods with the quantum principle of chemical reactions[31,32] related to well-known theories.[36−42] As long as the PES obtained by quantum chemical calculations has the same topography as the real PES with stable accuracies over the whole range, applications of the SHS method to GRRM in excited states or ionic states may also be promising for exploring uncultivated worlds of chemistry.

Acknowledgment. The present work has been financially supported by the Ministry of Education, Science, Sports, and Culture, by its Grants-in-Aid of Scientific Research No. 17655001, as well as a Grant-in-Aid for COE project, Giant Molecules and Complex System, 2004. S.M. is supported by a Research Fellowship of the Japan Society for Promotion of Science for Young Scientists.

Supporting Information Available: Tables of relative energies including zero point energy (ZPE) corrections and ZPE values (at 6-311++G** level of theory) for all stationary points included in global reaction route maps. This material is available free of charge via the Internet at http://pubs.acs.org.

References and Notes

(1) Mezey, P. G. *Potential energy hypersurfaces*; Elsevier: Amsterdam, New York, 1987.

(2) Jensen, F. *Introduction to Computational Chemistry*; Wiley: Chichester, UK, 1998.

(3) Schlegel, H. B. *J. Comput. Chem.* **2003**, *24*, 1514.

(4) Fukui, K. *Acc. Chem. Res.* **1981**, *14*, 363.

(5) Banerjee, A.; Adams, N.; Simons, J.; Shepard, R. *J. Phys. Chem.* **1985**, *89*, 52.

(6) Császár, P.; Pulay, P. *J. Mol. Struct.* **1984**, *114*, 31.

(7) Pancíř, J. *Collect. Czech. Chem. Commun.* **1975**, *40*, 1112.

(8) Cerjan, C. J.; Miller, W. H. *J. Chem. Phys.* **1981**, *75*, 2800.

(9) Simons, J.; Jørgensen, P.; Taylor, H.; Ozment, J. *J. Phys. Chem.* **1983**, *87*, 2745.

(10) Baker, J. *J. Comput. Chem.* **1986**, *7*, 385.

(11) Wales, D. J. *J. Chem. Phys.* **1994**, *101*, 3750.

(12) Munro, L. J.; Wales, D. *J. Phys. Rev. B* **1999**, *59*, 3969.

(13) Gotō, H. *Chem. Phys. Lett.* **1998**, *292*, 254.

(14) Tsai, C. J.; Jordan, K. D. *J. Phys. Chem.* **1993**, *97*, 11227.

(15) Basilevsky, M. V.; Shamov, A. G. *Chem. Phys.* **1981**, *60*, 347.

(16) Basilevsky, M. V. *Chem. Phys.* **1982**, *67*, 337.

(17) Rowe, D. J.; Ryman, A. *J. Math. Phys.* **1982**, *23*, 732.

(18) Hoffman, D. K.; Nord, R. S.; Ruedenberg, K. *Theor. Chim. Acta* **1986**, *69*, 265.

(19) Jørgensen, P.; Jensen, H. J. A.; Helgaker, T. *Theor. Chim. Acta* **1988**, *73*, 55.

(20) Quapp, W. *Theor. Chim. Acta* **1989**, *75*, 447.

(21) Schlegel, H. B. *Theor. Chim. Acta* **1992**, *83*, 15.

(22) Sun, J.-Q.; Ruedenberg, K. *J. Chem. Phys.* **1993**, *98*, 9707.

(23) Bondensgård, K.; Jensen, F. *J. Chem. Phys.* **1996**, *104*, 8025.

(24) Quapp, W.; Hirsch, M.; Imig, O.; Heidrich, D. *J. Comput. Chem.* **1998**, *19*, 1087.

(25) Quapp, W.; Hirsch, M.; Heidrich, D. *Theor. Chem. Acc.* **1998**, *100*, 285.

(26) Bofill, J. M.; Anglada, J. M. *Theor. Chem. Acc.* **2001**, *105*, 463.

(27) Crehuet, R.; Bofill, J. M.; Anglada, J. M. *Theor. Chem. Acc.* **2002**, *107*, 130.

(28) Hirsch, M.; Quapp, W. *J. Comput. Chem.* **2002**, *23*, 887.

(29) Dallos, M.; Lischka, H.; Monte, E. V. D.; Hirsch, M.; Quapp, W. *J. Comput. Chem.* **2002**, *23*, 576.

(30) Hirsch, M.; Quapp, W. *J. Mol. Struct.* (*THEOCHEM*) **2004**, *689*, 1.

(31) Ohno, K.; Maeda, S. *Chem. Phys. Lett.* **2004**, *384*, 277.

(32) Maeda, S.; Ohno, K. *J. Phys. Chem. A* **2005**, *109*, 5742.

(33) Hu, S.-W.; Lu, S.-M.; Wang, X.-Y. *J. Phys. Chem. A* **2004**, *108*, 8485.

(34) Goddard, J. D.; Yamaguchi, Y.; Schaefer, H. F., III *J. Chem. Phys.* **1992**, *96*, 1158.

(35) Aplincourt, P.; Henon, E.; Bohr, F.; Ruiz-López, M. F. *Chem. Phys.* **2002**, *285*, 221.

(36) Bell, R. P. *Proc. R. Soc. London, Ser. A* **1936**, *154*, 414.

(37) Evans, M. G.; Polanyi, M. *Trans. Faraday Soc.* **1936**, *32*, 1333.

(38) Hammond, G. S. *J. Am. Chem. Soc.* **1955**, *77*, 334.

(39) Woodward, R. B.; Hoffmann, R. *Angew. Chem., Int. Ed. Engl.* **1969**, *8*, 781.

(40) Fukui, K.; Yonezawa, T.; Shingu, H. *J. Chem. Phys.* **1952**, *20*, 722.

(41) Fleming, I. *Frontier Orbitals and Organic Chemical Reactions*; Wiley: London, UK, 1976.

(42) Marcus, R. A. *J. Phys. Chem.* **1968**, *72*, 891.

(43) Maeda, S.; Ohno, K. *Chem. Phys. Lett.* **2003**, *381*, 177.

(44) Maeda, S.; Ohno, K. *Chem. Phys. Lett.* **2005**, *404*, 95.

(45) Page, M.; McIver, J. W., Jr. *J. Chem. Phys.* **1988**, *88*, 922.

(46) Farkas, Ö.; Schlegel, H. B. *J. Chem. Phys.* **1999**, *111*, 10806.

(47) Broyden, C. G. *J. Inst. Math. Appl.* **1970**, *6*, 76. Fletcher, R. *Comput. J.* (*Switzerland*) **1970**, *13*, 317. Goldfarb, D. *Math. Comput.* **1970**, *24*, 23. Shanno, D. F. *Math. Comput.* **1970**, *24*, 647.

(48) Bofill, J. M. *J. Comput. Chem.* **1994**, *15*, 1.

(49) Frisch, M. J.; Trucks, G. W.; Schlegel, H. B.; Scuseria, G. E.; Robb, M. A.; Cheeseman, J. R.; Montgomery, J. A., Jr.; Vreven, T.; Kudin, K. N.; Burant, J. C.; Millam, J. M.; Iyengar, S. S.; Tomasi, J.; Barone, V.; Mennucci, B.; Cossi, M.; Scalmani, G.; Rega, N.; Petersson, G. A.; Nakatsuji, H.; Hada, M.; Ehara, M.; Toyota, K.; Fukuda, R.; Hasegawa, J.; Ishida, M.; Nakajima, T.; Honda, Y.; Kitao, O.; Nakai, H.; Klene, M.; Li, X.; Knox, J. E.; Hratchian, H. P.; Cross, J. B.; Adamo, C.; Jaramillo, J.; Gomperts, R.; Stratmann, R. E.; Yazyev, O.; Austin, A. J.; Cammi, R.; Pomelli, C.; Ochterski, J. W.; Ayala, P. Y.; Morokuma, K.; Voth, G. A.; Salvador, P.; Dannenberg, J. J.; Zakrzewski, V. G.; Dapprich, S.; Daniels, A. D.; Strain, M. C.; Farkas, O.; Malick, D. K.; Rabuck, A. D.; Raghavachari, K.; Foresman, J. B.; Ortiz, J. V.; Cui, Q.; Baboul, A. G.; Clifford, S.; Cioslowski, J.; Stefanov, B. B.; Liu, G.; Liashenko, A.; Piskorz, P.; Komaromi, I.; Martin, R. L.; Fox, D. J.; Keith, T.; Al-Laham, M. A.; Peng, C. Y.; Nanayakkara, A.; Challacombe, M.; Gill, P. M. W.; Johnson, B.; Chen, W.; Wong, M. W.; Gonzalez, C.; Pople, J. A. *GAUSSIAN 03*, Revision C.02,; Gaussian, Inc.: Wallingford, CT, 2004.

(50) Koga, N.; Morokuma, K. *Chem. Rev.* **1991**, *91*, 823.

(51) Blomberg, M. R. A.; Karlsson, C. A. M.; Siegbahn, P. E. M. *J. Phys. Chem.* **1993**, *97*, 9341.

(52) Niu, S.; Hall, M. B. *Chem. Rev.* **2000**, *100*, 353.

(53) Wang, Y.-G.; Sun, C.-J.; Deng, C.-H. *J. Mol. Struct.* (*THEOCHEM*) **1998**, *429*, 207.

(54) Wang, Y.-G.; Sun, C.-J.; Deng, C.-H. *J. Phys. Chem. A* **1998**, *102*, 5816.

(55) Bauschlicher, C. W., Jr. *Chem. Phys. Lett.* **1994**, *229*, 577.

(56) Bera, J. K.; Samuelson, A. G.; Chandrasekhar, J. *Organometallics* **1998**, *17*, 4136.

(57) Hermann, H. L.; Boche, G.; Schwerdtfeger, P. *Chem. Eur. J.* **2001**, *7*, 5333.

(58) Trost, B. M. *Science* **1991**, *254*, 1471.

(59) Trost, B. M. *Angew. Chem., Int. Ed. Engl.* **1995**, *34*, 259.

(60) Collins, T. J. *Science* **2001**, *291*, 48.

(61) Collins, T. J. *Acc. Chem. Res.* **2002**, *35*, 782.

(62) Wang, Z.-X.; Manojkumar, T. K.; Wannere, C.; Schleyer, P. v. R. *Org. Lett.* **2001**, *3*, 1249.

(63) Kaufmann, E.; Sieber, S.; Schleyer, P. v. R. *J. Am. Chem. Soc.* **1989**, *111*, 4005.

(64) Maeda, S.; Ohno, K. *Chem. Lett.* **2004**, *33*, 1372.

(65) Maeda, S.; Ohno, K. *Chem. Phys. Lett.* **2004**, *398*, 240.